

# RHEOLOGICAL PROPERTIES COMPARISON OF AQUEOUS DISPERSED NANOCELLULOSE DERIVED FROM A NOVEL PATHWAY-PRODUCED MICROCRYSTALLINE CELLULOSE OR BY CONVENTIONAL METHODS

KATARINA DIMIC-MISIC<sup>1</sup>, KARI VANHATALO<sup>1,3</sup>, OLLI DAHL<sup>1</sup>, PATRICK GANE<sup>1,2</sup>

<sup>1</sup>Aalto University, Department of Bioproducts and Biosystems, School of Chemical Engineering, Aalto-Yliopisto 16400, Finland

<sup>2</sup>Omya International AG, Baslerstrasse 42, 4665 Oftringen, Switzerland

<sup>3</sup>Andritz Oy, Tammasaarenkatu 1, 00180 Helsinki, Finland

\*Corresponding author: [katarina.dimic.misic@aalto.fi](mailto:katarina.dimic.misic@aalto.fi)

Received: 6.7.2018, Final version: 5.9.2018

## ABSTRACT:

Novel-produced never-dried and dried microcrystalline cellulose (MCC) was previously compared with a commercial MCC. The novel MCC was shown to be a suitable starting material for producing cellulose nanofibrils, in turn having similar molecular weight  $M_w$ , crystallinity, and particle size comparable to those from sequentially enzymatic and mechanically treated softwood sulphite pulp, but at lower cost. The study here presents a rheological parameterisation of the aqueous suspension throughout the process, aimed at delivering a correlation between specific surface area, at equal material particle size, and adsorptive coupling between neighbouring cellulose particles and interstitial water under flow. We conclude that combining dynamic viscosity with an independent measure of particle size provides a suitable quality control of MCC-derived cellulose nanofibrils, obviating the need for individual property-raw material relationships to be evaluated, and this principle may provide a generalised method for use in the production of cellulose nanofibrils.

## KEY WORDS:

Microcrystalline cellulose, micro nanofibrillar cellulose, nanocellulose, cellulose-water interaction under flow, quality parameterisation, surface area-rheology response

## 1 INTRODUCTION

Renewable and biodegradable cellulose-based materials have shown promise for various potential applications including replacement of fossil oil-based products due to their excellent functional properties [1, 2]. Cellulose microfibrils consist of both amorphous and crystalline regions, and this structure of native cellulosic fibres enables the production of two distinct families of micro and nanocellulose materials with different morphological and rheological properties [3, 4]. Treatment of them in strongly acidic conditions leads to an extensive hydrolysis of the amorphous fraction leading to the release of short rod-like cellulose particles with high crystallinity and low aspect ratio, termed microcrystalline cellulose (MCC) [1, 5]. Alternatively, when macroscopic cellulose fibres are mechanically disintegrated, avoiding the strongly acidic conditions, long nanoscale diameter, partly amorphous, fibrils are produced [6, 7]. In the literature, terms such as microfibrillated cellulose

(MFC), nanofibrillated cellulose (NFC), cellulose nanofibres/fibrils (CNF), and, at intermediate energy input, a product termed micro nanofibrillated cellulose (MNFC), in which the microfibrils display nanofibrils on their surface are used [1, 5].

Micro and nanofibrillated cellulose have been demonstrated positively in many applications related to their functional properties, such as high surface area, high bonding strength, biodegradability, or low density [5–7]. The nanofibrils in both NFC and MNFC are typically 4–20 nm in diameter and 500–2000 nm in length [1, 3]. The aqueous suspension properties are influenced by hydrogen bonding between nanofibrils and water molecules and have rheological properties displaying partial gel-like structure [3, 5, 8]. Due to the high aspect ratio and easily modifiable surface chemistry, MNFC has high potential to act as a building block for various applications including reinforcement in polymer matrices, aerogels, foams, nanopaper, and transparent and flexible films [7, 9]. When dispersed in water, these highly

surface charged fibrils form a stable dispersed transparent or semi-opaque gel-like suspension, depending on the number of remaining larger particles at concentrations as low as 0.03 % [10–14]. Mechanical production of MNFC utilises high-pressure homogenisers or fluidisers, in a process where the cell walls of cellulose containing fibres are delaminated and the nano-sized cellulose fibrils are liberated. The process is, nonetheless, extremely energy intensive and, furthermore, high pressure homogenisers and fluidisers are easily clogged by the natural fibres comprising the cellulosic feed, some of which are retained also after processing [15, 16]. To minimise these drawbacks, the natural fibres are often pre-treated using various mechanical/enzymatic treatments, oxidation, and introduction of charges [17–20]. The production yield through acid hydrolysis is typically only 50–60 % due to solubilisation of amorphous regions upon hydrolysis [21–24]. Although chemical pre-treatments of pulp significantly lower the energy consumption in NFC production, it nonetheless remains the greatest challenge to match the cost-performance criteria due to increasing complexity of these methods, there remains a need for further development of economical and sustainable methods for producing such fibrillar materials [19–21].

The gel-like MCC and NFC suspensions have a high water content, which increases transportation costs and reduces their processability. Furthermore, during storage, the aqueous environment serves to support the growth of undesirable microorganisms [1, 3, 9]. Such economic and technical disadvantages continue to drive innovation toward obtaining nanoscale cellulose products with less water [2, 3, 25]. Generally, the direction of investigation has been toward improving dewatering of the nanocellulose. In addition to the challenges in production and commercialisation of lower water content nanofibrillar materials, there are time-dependent material property changes to consider, such as hornification; the irreversible formation of hydrogen bonds between fibrils during suspension dehydration [26–28]. Alternatively, among the various techniques for obtaining dry MNFC particles, spray drying of MNFC suspensions is found to be a versatile technique that offers advantages due to rapid heat and mass transfer in a continuous mode. MCC has been a subject of research over the past 60 years [24, 29, 30]. It is to be found already in the market and is nowadays used for a range of high-value applications, such as cosmetics, dairy, food and pharmaceuticals [1, 2, 24]. Contrary to the typical high aspect ratio microfibrillar starting material, MCC obtained by subjecting cellulose fibres to extensive acid hydrolysis has low aspect ratio, which leads to low suspension viscosity. Some early fibrillation studies with MCC were made to clarify its propensity to break up into single colloidal par-

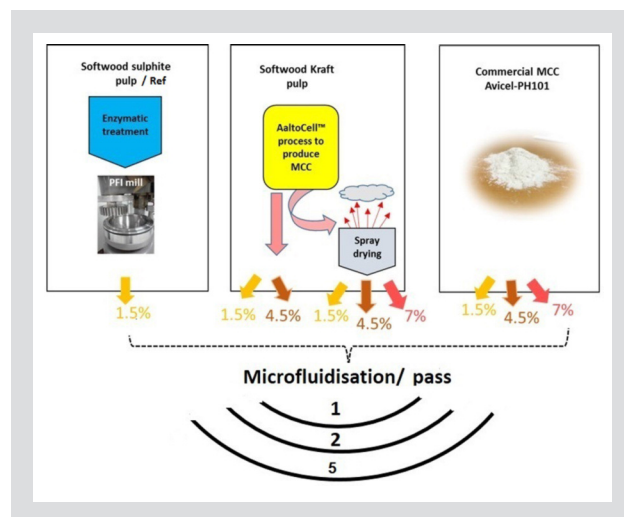


Figure 1: Production of (M)NFC and CNF suspensions via different routes as a function of feed material and increasing fluidising cycles: 1, 2, and up to 5 passes.

ticles under mechanical shear [31]. However, if a dry MCC could in turn decrease logistics cost and provide for a significant increase in feed consistency to a high-pressure homogeniser (HPH), then the production cost of highly crystalline MNFC fibrillar material, derived from it, could be made extremely attractive [32, 33]. Furthermore, if it were possible to design a process to produce lower cost MCC, then even greater advantage could be derived. Such process was described recently in the literature (AaltoCell™) where a low chemical consumption raw material, such as Kraft pulp, and is being considered as a component process line in biorefining [33–37].

A major challenge in making a rheological analysis of MNFC suspensions in general is apparent wall-slip, arising from a solids depleted layer forming in contact with the geometry wall having, thus, a significantly lower viscosity than the bulk suspension. The use of serrated surfaces in plate-plate geometry or the adoption of a vane spindle in the bob-in-cup geometry serve to decrease the apparent wall-slip effect, and in turn shear-banding [38]. Additionally, the application of shear in fibril suspensions is found to induce changes in flocculation and agglomeration of the fibrils, effects that are consistency dependent, and which vary in respect to the morphology and surface charge of the nanofibrils [39]. In the light of recent understanding, rheological evaluation of such suspensions has become an important tool for the investigation of nanocellulose processability, where even very small alterations in the production routes result in large effects on rheological behavior and dewatering, related often to minor changes in nanofibril morphology, surface charge or crystallinity [39–41]. We compare rheologically [41–43] nanocellulose fibril suspensions obtained from MCC, comparing material produced from commercially available MCC with material produced from the novel lower cost MCC production route, derived from Kraft pulp, and in turn with reference material derived from enzymatically treated sulphite bleached pulp [44, 45]. The results show close similarity.

## 2 EXPERIMENTAL

### 2.1 MATERIALS AND METHODS

#### 2.1.1 MCCs as raw material and comparison with sulphite pulp

In this work, we evaluate the rheological properties of cellulose nanofibrils produced by high pressure fluidising of three raw materials, produced either (i) by enzymatic treatment of never dried sulphite pulp (traditional mechanical route to NFC/MNFC route) [17, 18] or (ii) via the AaltoCell™ lower cost MCC route from softwood Kraft pulp (resulting in a highly crystalline cellulose nanofibrillar material - NFC) [30], and (iii) commercially available MCC derived from cotton fibre as feed material [29, 32]. The three respective routes are shown schematically in Figure 1. The cotton-derived commercial MCC Avicel® PH-101, purchased from Sigma-Aldrich (Germany) was used in refining steps without pretreatment. Two different softwood chemical pulps were used for preparation of the other raw materials: a bleached sulphate pulp from a Central Finnish pulp mill for the MCC and a bleached sulphite pulp (Domsjö ECO Bright, Domsjö Fabriker AB, Sweden) for the reference material. The employed sulphuric and citric acids, and disodium hydrogen phosphate were all analytical grade, purchased from Sigma-Aldrich (St. Louis, USA), and used without further purification. The commercial endoglucanase enzyme used was EcoPulp R® (RAOL Oy, Finland) with an activity of 152 000 CMU/g (cellulose tubule uncoupling protein). The enzyme solution was diluted prior to hydrolysis. Distilled water was used in all laboratory procedures.

#### 2.1.2 Preparation of reference raw material

The reference raw material (“Ref.” in the following) was prepared following the previously reported procedure [30, 32]. In brief, a commercial bleached softwood sulphite pulp was refined to a Schopper-Riegler value of 28° by PFI milling, employing the standards ISO 5264-2:2011 and ISO 5267-1:1999. The subsequent enzymatic treatment used an enzyme charge of 500 CMU/g at 50°C at 4% cellulose consistency and gentle spoon mixing every

20 min for 2 h 20 min [39, 45]. The treatment was made in citric acid (0.1 M) and a disodium hydrogen phosphate (0.2 M) buffer solution, adjusting the pH to 4.8. After the incubation period, the fibres were washed in a Büchner funnel until wash filtrate conductivity was 5 µS. The enzymatic activity was discontinued by incubating the 4% pulp at 90 °C for 30 min with a subsequent washing step. Finally, the pulp was mechanically refined to a Schopper-Riegler value of 85°, again using the PFI mill, according to ISO 5264-2:2011 and ISO 5267-1:1999.

#### 2.1.3 Preparation of MCC raw material (never-dried and spray dried)

The procedure described by Dahl et al. [27] was used to manufacture the MCC raw materials via the AaltoCell™ process. A bleached softwood sulphate pulp was hydrolysed in a tube-like 2.5 dm<sup>3</sup> metal reactor by using H<sub>2</sub>SO<sub>4</sub> as hydrolysing agent. An acid charge of 1.5%, calculated based on oven-dry cellulose in 10% consistency pulp suspension was maintained at 160 °C. Hydrolysis was ended when the degree of polymerisation (DP) reached a level of 390 by cooling the reactor to room temperature and washing the MCC produced in a Büchner funnel on a 90-mesh wire sieve. A portion of the MCC was retained as never-dried product and used as such in the further experiments to produce CNF (referred to as “DP390” in the following) [45]. The remaining part of the produced MCC was converted to dry powder (referred to as “DP390-dry” in the following) by spray drying (Niro Mobile Minor, Niro Atomizer Ltd., Copenhagen, Denmark) at 5% feed consistency using inlet and outlet air temperatures of 350 and 90°C, respectively. The MCC so produced typically contains about 10% xylan, the rest being highly crystalline cellulose.

#### 2.1.4 Preparation of (M)NFC and CNF

The microfluidising equipment (Microfluidiser M-110P, Microfluidics Corp.) consisted of two Y-shaped impact chambers connected in series [30]. The internal diameter of the first impact chamber flow channel was 200 µm and the second 100 µm. The production pressure was controlled at 2000 bar throughout to prepare all the products, ranging from micro to nanofibrillated cellulose (M)NFC via the reference route, and cellulosic micro to nanofibrillar (CNF) via the MCC route according to the number of fluidising passes applied. After each pass through the impact chambers a sample was taken for further analysis. The maximum number of passes was five. Various feed consistency levels for each raw material

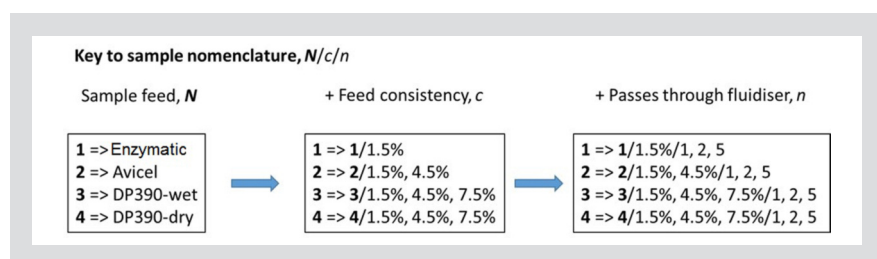


Figure 2: Sample labelling.

were tried and the maximum consistency levels were determined according to the operation of the fluidiser equipment, i.e. the maximum consistency possible whilst maintaining a smooth and trouble-free flow-through, implying no uncontrollable thickening, clogging or other processing problems [21, 31]. The applicable sample nomenclature including feed type to the fluidiser, consistency and number of passes (N/c/n) is shown in the schematic in Figure 2.

## 2.2 ANALYTICAL TOOLS

### 2.2.1 Particle size and morphology

The particle/agglomerate size distributions of the MCCs (Avicel, DP390 never-dried and DP390-dry) were measured in triplicate using a Mastersizer 2000 equipped with a Hydro 2000 MU dispersion unit (Malvern Instrument Ltd, United Kingdom) [30]. The volume fraction size distribution median diameter  $d_{50v}$  value was used as a measure of the applicable particle size. The following measurement protocol and parameters were used as described previously [32]. About ~ 0.5 g of the sample solid was mixed into 25.0 cm<sup>3</sup> of water using a dispersion unit at 800 1/min (rpm) stirring rate. Next the suspension was ultrasonicated for 60 s with an amplitude of 39 % and frequency of 20 Hz. A fully disintegrated sample (5 cm<sup>3</sup>) was pipetted into the dispersion unit and the particle size distribution was measured by three sequential five-second measurements at 60 s intervals. The background signal was determined with distilled water alone each time prior to sample measurement. The Ref. sample fibre morphology was analysed by a Kaajaani FiberLab<sup>TM</sup> (Metso Automation Oy, Finland). A sample was diluted to 0.004 % consistency using distilled water. The analyser set measurement throughput speed was 25 fibres 1/s and the sample volume included at least 40000 fibres. The measurements were once again performed in triplicate.

### 2.2.2 Degree of hydrolysis polymerisation (DP)

The DP was calculated from the intrinsic viscosity  $[\eta]$  of the cellulose raw materials measured according to SCAN-C 15:99. The calculation was made according to the standard SCAN-C 15:88 Mark-Houwink equation, employing previously published constants

$$[\eta] = Q'(DP)^a \quad (1)$$

where  $[\eta]$  represents the intrinsic viscosity, and  $Q'$  and  $a$  have the values 0.42 and 1.0, respectively, assuming a DP of < 950 and the values 2.28 and 0.76 if DP > 950 [32, 33]. All measurements were repeated in triplicate.

### 2.2.3 Electron microscopy

Scanning electron micrographs (SEM) of the raw materials and the products were taken by field-emission scanning electron microscopy (FE-SEM: Philips XL 30 Feg, Cryo: Alto 2500, EDX: Inca, Oxford Instruments with AZtec software) [42]. The wet samples were subjected to two-step liquid-displacement using a fully water-soluble low-molecular weight alcohol, frozen and then allowed to sublimate under freeze-drying conditions. Prior to FE-SEM imaging, the samples were coated with platinum.

### 2.2.4 Specific surface area

The specific surface area (SSA) of the samples was analysed using a NOVA 4000 (Quantachrome GmbH and Co., Odelzhausen, Germany) and pure N<sub>2</sub> gas to provide adsorption isotherms. SSA was then calculated by the Brunauer–Emmett–Teller (BET) equation [33, 46]. The sample pre-treatment procedure was identical to that used in SEM imaging.

### 2.2.5 Crystallinity

X-ray powder diffraction (XRD) patterns (see Appendix Figure A1) were obtained on an X'Pert PRO MPD Alpha-1 diffractometer (PANalytical, Almelo, Netherlands) using a Ge-filtered CuK $\alpha$  radiation beam ( $\lambda = 0.154056$  nm) operated at 45 kV and 40 mA. The samples were measured at a scan rate of 0.033667° 1/s over a  $2\theta$ -range of 5–70°. Prior to XRD measurements, the cellulose raw material samples were air-dried for 24 h at room temperature, followed by 12 h at 80 °C. The wet samples were first poured onto a laboratory Petri dish before drying using the same procedure. The crystallinity index (CI) was calculated by the peak height method from the XRD data, according to the equation by Segal et al [47, 48]:

$$CI = 100 \frac{I_{002} - I_{am}}{I_{002}} \quad (2)$$

where  $I_{002}$  is the intensity of the diffraction peak with Miller indices  $\{hkl\} = \{002\}$  in the crystalline region and  $I_{am}$  is the intensity of the background amorphous hump underlying the  $\{002\}$  diffraction peak, i.e. at  $2\theta(I_{002})$ . The cellulose crystallite size  $D_{hkl}$  was calculated from the width of the peak at  $2\theta$  around 22.4° adopting the Scherrer equation [61]

$$D_{hkl} = \frac{k'\lambda}{\beta \cos \theta} \quad (3)$$

where  $k'$  is the Scherrer constant (0.94),  $\lambda$  is X-ray wavelength,  $\beta$  is the full-width at half-maximum in radians, and  $\theta$  is the Bragg angle.

### 2.2.6 Turbidity

The sample suspension turbidity ( $=1/\text{light transmittance}$ ) was measured using a spectrophotometer (Shimadzu UV-1800 UV-VIS, Shimadzu Corporation, Japan) at 0.1 % solids consistency, as described by Kangas et al. [50] with the following modifications. The product sample was first dispersed in Milli-Q water by magnetic stirring at 300 1/min(rpm) for 15 min, followed by 1 min high-shear mixing at 4000 1/min (IKA T25 Ultra Turrax, Ika Labortechnik, Germany). Immediately after mixing each sample was analysed for light transmittance ( $\lambda = 200-1000$  nm). Transmittance was recorded at 600, 800, and 1000 nm. All measurements were repeated in triplicate.

### 2.2.7 Water retention value

A modified Water Retention Value (WRV) measurement was used in estimating the network level swelling of the product samples [32, 36]. The method has been developed from the standard SCAN-C 62:00, which includes centrifugation of the pulp pad at 3000 g for 15 min. Since the standard method is not suitable for pure MNFC suspensions, a mixture of 90 % never-dried bleached hardwood ( $WRV_0 = 1.8 \text{ cm}^3/\text{g}$ ) with 10 % (dry solids equivalent) of the sample to be analysed was used in the measurements, to promote sufficient drainage. The desired WRV of the sample is then calculated from the measured WRV of the mixture

$$WRV = \frac{WRV_{mix} - WRV_0 \cdot 0.9}{0.1} / \text{cm}^3 \text{g}^{-1} \quad (4)$$

## 2.3 RHEOLOGICAL MEASUREMENTS

### 2.3.1 Viscoelastic properties

A rotational and oscillation rheometer (Physica MCR 300) was used in both controlled shear and strain modes with a plate-plate geometry. The rheometer was equipped with roughened (serrated) top (PP20) and bottom (P-PTD 200) plates [3, 11]. The bottom plate implementing a Peltier temperature control with fixed temperature at 23 °C. The gap between plates was initialised to 2.5 mm [12]. The linear viscoelastic behavior was identified with oscillatory measurements applying a strain sweep at a constant angular frequency  $\omega$  of 10 rad/s, after which frequency sweep measurements were performed where the strain  $\gamma$  was varied between 0.01 to 500 % [11]. It should be noted here that for macrofibrillar as well as colloidal particulates that undergo multiple structural configuration changes generating a variety of elastic interactions viscoelastic re-

sponse to deformation does not occur over a single linear viscoelastic region (LVE), and so the term LVE in this context refers to the region applicable for the fixed frequency of oscillation used, providing values for the viscoelastic moduli ( $G'$  as storage and  $G''$  as loss modulus) [36, 37].

### 2.3.2 Yield stress

Yield stress is perhaps the most important rheological property of complex suspensions, as it needs to be exceeded in order that flow takes place. As the apparent effective yield stress depends on the determination method and the flow geometry, it can be distorted by potential wall-slip, or better defined as solids depletion at the geometrical boundary, in gel-like materials, which adds to the challenge of its estimation [36, 42]. Due to the different nature of yield stress phenomena within nanofibrillar suspension systems, related to water binding and gelation properties as well as particle morphology/aspect ratio, we evaluated yield stress using results from viscoelastic measurements [39, 43]. The elastic stress component in oscillatory measurements is given by

$$\tau_s = G' \gamma \quad (5)$$

As strain  $\gamma$  is increased at a constant rate under constant frequency  $\omega$  in the oscillatory amplitude sweep measurements, the maximum in the elastic stress  $\tau_s$  corresponding to the static elastic yield stress  $\tau_s^0$  was determined as the first point of deviation from the linear elastic deformation occurring at a corresponding critical strain value  $\gamma_c$ .

### 2.3.3 Shear thinning behavior

The influence of shear rate on the variation of complex viscosity  $\eta^*$  was evaluated by measuring complex viscosity response as a function of increasing angular frequency  $\omega$  in the range of 0.1–100 rad/s. To define differences between the respective suspensions regarding their colloidal interactions, packing effects and friction between particles and/or nanofibrils during the flow, flow curves of the complex viscosity  $\eta^*$  were also fitted to a power law according to an equivalent of the Ostwald-de Waele empirical model (Equation 7) allowing in particular for the comparison of different water binding properties within the linear viscoelastic region (LVE) for an effective complex viscosity  $\eta^*$ , using an effective shear rate determined as the root mean square value under oscillation, and effective dynamic viscosity beyond the elastic region  $\eta$ , respectively [39, 40]. For a sinusoidal oscillation with angular frequency  $\omega$  (Figure 3) the root mean square velocity is given by

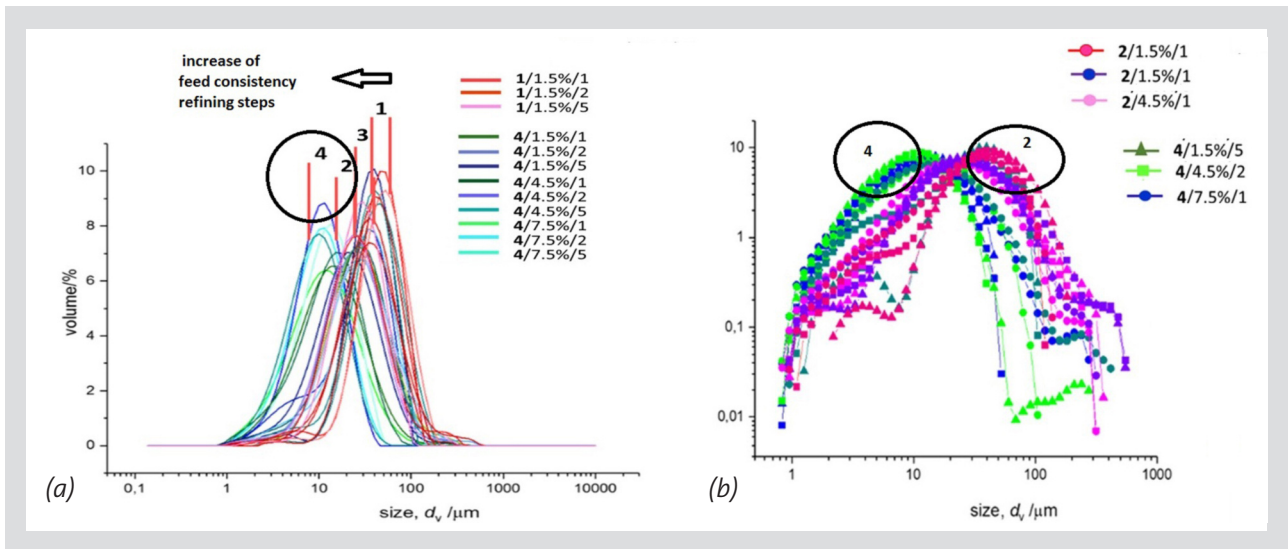


Figure 3: The volume equivalent agglomerate particle size distribution as measured using light scattering of feed materials prior to fluidising (a) and example products after 1, 2, and 5 fluidising passes comparing 3 => DP390-wet and 4 => DP390-dry at three different feed solids concentrations (b).

$$v_{rms} = \frac{\sqrt{2}}{\pi} \omega A_o \quad (6)$$

where  $A_o$  is the amplitude of the oscillation. We can, therefore, derive a root mean square shear rate  $\dot{\gamma} = v_{rms}/A_o$  such that the Ostwald-de Waele shear thinning model can be approximated in the case of complex viscosity as

$$\eta^* = k_c (\dot{\gamma}_{rms})^{n_c-1} = k_c \left( \frac{\sqrt{2}}{\pi} \omega \right)^{n_c-1} \quad (7)$$

where  $k_c$  and  $n_c$  in Equation 7 are the flow consistency index and the power-law exponent, respectively. For the complex viscoelastic case  $n_c = 1$  indicates a Newtonian fluid, whereas  $n_c < 1$  indicates a pseudo-plastic (shear thinning) behavior.

### 2.3.4 Structure recovery 3ITT measurements

The purpose of this recovery measurement is to determine how consistency and presence of a large number of fine fibrils might lead to induced flocculation/agglomeration within the gel-like sample matrix and so affect recovery of network structure after removal of high shear [39, 51]. This measurement can be expected to provide information on the dynamic elastic structure recovery after high shear deformation in a head box and/or during fluidising. It is desirable that the initially high dynamic viscosity can perhaps be reduced to provide an easily “flowing state” for application and then to recover when forming the final material. Initially, in the first low shear interval, samples were subjected to low shear rate under purely rotational conditions ( $\dot{\gamma} = 0.11/s$ ), then subsequently high shear rate ( $\dot{\gamma} = 500 1/s$ ) and finally once again low shear rate “recovery” ( $\dot{\gamma} = 0.1$

$1/s$ ). Structure recovery was traced in respect to recovery of dynamic transient viscosity  $\eta^+$  in the third interval, expressed as percentage of ratio  $\eta^+/\eta_o$  after 300 s of measurements, where  $\eta_o$  is the low shear viscosity at the beginning of the first interval [51, 52].

### 2.3.5 Rheological data variation

Data variation in the rheological measurement for the gel-like thixotropic systems was within 10%. Noise reduction in the raw data was additionally applied using Tikhonov regularisation [42]. The first step in the correction process is to remove obvious outliers (negative values and values out of scale) [37, 38]. The actual Tikhonov regularisation step consists of minimising a linear combination of a residual term (between raw and smoothed data) and a term representing the amount of remaining noise in the smoothed data. Adjusting the ratio between the coefficients in the linear combination determines the level of smoothness of the smoothed data. Fitting low order polynomials to the ends of the data and replacing the y-coordinates of the ends with values calculated from the fits prevents the appearance of unnecessary winding at the ends. If necessary, the smoothing procedure could be advanced segmentally.

## 3 RESULTS AND DISCUSSION

### 3.1 PARTICLE PROPERTIES

#### 3.1.1 Size distribution – feed and product

The differences between the raw materials and the resulting fluidised products, regarding physical size can be observed from the laser light scattering agglomerate size distribution presented in Figure 3. The size distributions of the feed material are shown in the plot Figure 3a. They fall into four categories of decreasing agglomerate size (1) Ref. fibrous source, (3) DP390-wet, (2) com-

mercially sourced powder MCC, and (4) DP390-dry. Remembering that the measurement records a volume average scattering cross-section, it is not easy to extract shape information, which becomes immediately revealed when viewing the electron microscope images (Figure 4) [53]. However, the order of size fully reflects the source material, such as the fibre-nature of the enzymatically treated pulp 1 being the largest [32], as well as differences in sample preparation for the DP390-wet [30, 33] and DP390-dry samples [54], since we can expect some collapse of nanofibrils during drying and thus similar in properties to those of the commercial powder MCC. Therefore, it is possible even at this stage to speculate that drying reduces the surface material extension into the aqueous phase that takes place in such hydrophilic highly charged species. Figure 3b also clearly shows that the ability to raise solids concentration of the feed when using dried MCC results in finer product material, and interestingly the action of drying the MCC (DP390-dry) also delivers an even finer end-product [32, 54].

### 3.1.2 Particle morphology – feed and product

Figure 4 shows the SEM images of the raw feed materials, and the data can be compared with Figure 3a. Clear differences are visible between the materials when comparing the enzymatically treated bleached fibre 1 (Figure 4a) and the MCC rod-like materials 2, 3, and 4 (Figure 4b–d). However, closer inspection also reveals some significant structural differences between the commercial Avicel MCC 2 and the MCCs produced using the AaltoCell process 3 and 4 (Figure 4b versus Figures 4c and d). The AaltoCell DP390 material 3 and 4 displays significantly larger aspect ratio than the commercial MCC 2, which probably reflects to some extent the softwood Kraft pulp source properties [30, 32, 33]. Importantly, we can observe the impact of drying on the DP390-dry 4 versus DP390-wet MCC 3, and by implication also the commercial dry powder 2, in that the surface microfibrillar structure, seen in the wet state and preserved during the solvent exchange sample preparation for the microscope imaging, has collapsed onto the parent particle

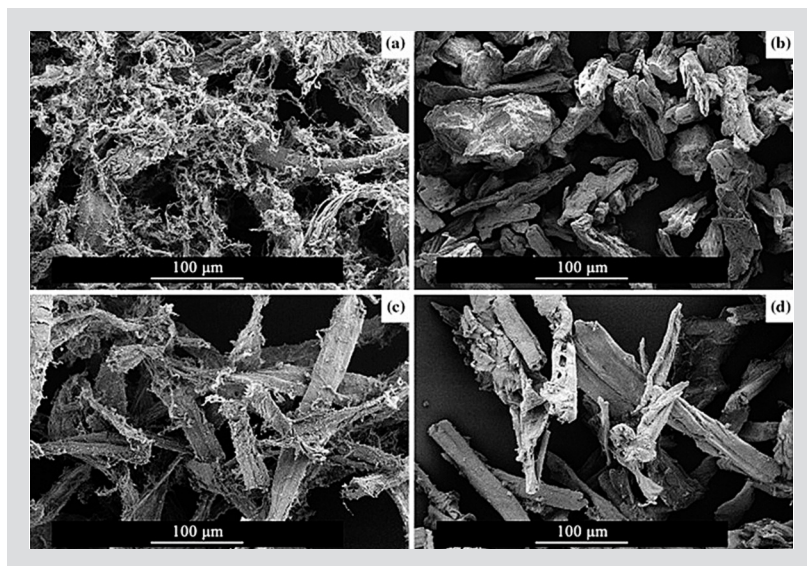


Figure 4: SEM images of feed samples prior to fluidising: (a) Enzymatically pre-treated reference sample (1 => Ref), (b) cotton linters-originated powder MCC (2 => Avicel), (c) AaltoCell<sup>TM</sup> originated 3 => DP390-wet MCC, solvent exchanged for imaging, and (d) spray dried 4 => DP390-dry MCC.

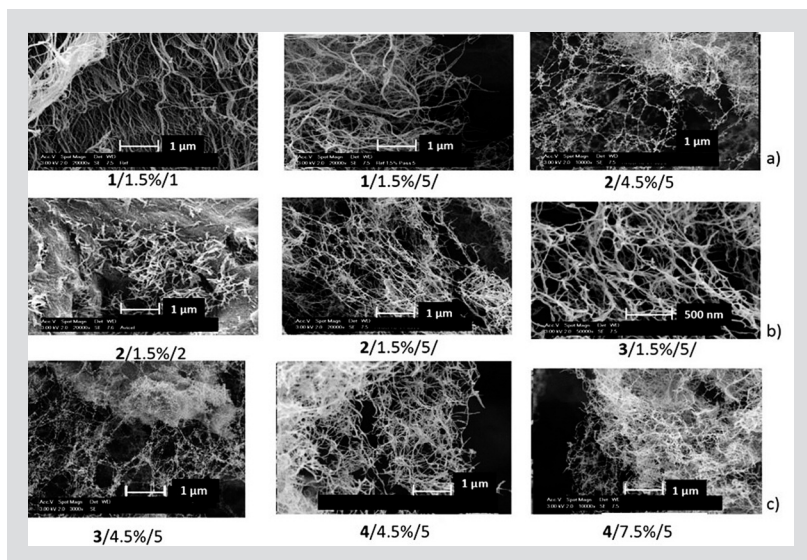


Figure 5: SEM images revealing the difference in the morphology of fibrillated product regarding the feed type, consistency and fluidising passes: (a) 1 and 2 => Ref fibre-derived and Avicel, and (b) 2 and 3 => Avicel and wet DP390-wet and (c) 3 and 4 => DP390, and spray dried DP390-dry MCC-derived products.

during the spray drying process, indicating the effect of meniscus forces during drying [32, 54]. This, then, agrees fully with the ranking of particle size seen in Figure 3a. Therefore, the properties of these DP390 MCC types, never-dried 3 versus spray dried 4, can be expected to differ prior to further processing [55].

The SEM images in Figure 5 show by taking selected examples that progressive passes through the high-pressure fluidiser and increasing feed consistency act to produce finer, and thinner, fibrillar structures as well as a more uniform fibril morphology [56]. Feeding consistency of 1.5 %, with one cycle of fluidising only, appears ineffective in producing fine nanostructure, such that higher consistency and greater fluidising are re-

quired to impart significant fibrillation [57]. Moreover, the micrographs indicate visually that there are small but nonetheless likely significant differences between the products processed from the two different DP390 MCC raw materials at the same feed consistency, recalling Figures 4c and d, namely never-dried DP390-wet MCC 3 and spray dried DP390-dry MCC 4, respectively, especially where higher process consistency (4.5 %) resulted in fibril structures displaying a very thinly fine “spider’s web”-like nature, with the dried MCC DP390-dry showing somewhat less entangled and slightly finer structures. Whether this hypothesis is statistically supportable should be revealed in the rheological behavior [57]. The SEM visual assessment, therefore is supported by the dynamic laser light scattering particle size results (Figure 3) and shows us by the inclusion of the results for increasing amount of feed consistency per fluidising steps, that increase in feed consistency behaves similarly to the increase in fluidising steps [31, 37, 56]. However, due to the large initial size of Ref fibre-derived feed particles 1, the feed consistency is limited to 1.5 %, which makes it impossible to reach the finer structure (Figure 5) and smaller size achievable using MCC as starting material.

The commercial MCC particles 2 showed similar surface texture as the spray-dried DP390-dry 4 samples, which indicates that hornification upon spray drying results in a decreased particle size MCC (Figure 3) as also seen corresponding to the SEM images (Figure 4) [35]. The given DP and Mw values are shown in Table 1 together with specific surface area (SSA). In general, SSA decreases upon acid hydrolysis, as manifest when going from feed sample Ref 1 towards wet MCC 3, and spray dried MCC 2 and 4, the latter spray dried DP390-dry 4 having similar SSA value as the commercial MCC 2: This effect also remains to be confirmed in the rheological characteristics. Crystallinity index (CI) results confirm that morphological similarities from SEM images seen in Figure 4 between Avicel MCC and DP390-dry MCC are also present in their solid molecular structure, as observed for similar materials in Vanhatalo et al. [32]. The SEM micrographs in the current study (Figure 5) are in good agreement with previous studies reporting fine cellulose fibrils of nanoscale dimensions after mechanical fibrillation [8, 11, 30].

### 3.2 RHEOLOGICAL PROPERTIES

#### 3.2.1 Viscoelastic behavior

The rheology of fibrillated cellulose suspensions is known to be dependent on the fines contained in the sample, associated with surface charge and fibril morphology, which are expected to influence suspension properties due to different friction and relative mobility

within the composite matrix [3, 13]. Therefore, it is necessary to decouple the effects of the combined drivers for these properties, namely feed consistency and number of passes through the fluidiser, e.g. for the same feed consistency, increased fluidising will change the level of fibrillation and determine the fibril morphology, whereas increased consistency at a fixed number of fluidising passes will increase the work input per pass and so increase fibrillation but likely modify the morphology [8, 56, 57]. Any differences in the degree of entanglement, agglomeration and/or flocculation in the network structure, resulting from the increased degree of fibrillation, should manifest itself in a change of suspension mechanical and viscoelastic properties, including gelation [39]. It is known that for gel-like nanocellulose suspensions  $G'$  and  $G''$  are relatively independent of angular frequency  $\sim \omega^0$ , while for viscoelastic materials both  $G'$  and  $G''$  have characteristic frequency dependency  $\sim \omega^n$  and for flocculated suspensions  $n_{G''} > n_{G'}$  [12, 56].

At the beginning of the strain sweep, under low strain  $\gamma$  (Figure 6) both storage and loss moduli exhibit a constant value ( $G_o'$  and  $G_o''$ ) with  $G_o' > G_o''$  until a critical strain amplitude  $\gamma_c$  is reached, which defines the end of the linear viscoelastic region (LVE). On the one hand, the change in extent of this span of constant moduli over strain (LVE) is visible for the MCC materials 2, 3, and 4, being greater for higher feed consistency and number of passes through the fluidiser [2, 57]. This reflects the increase of surface area and the greater number of thinner fibrils leading to a strong homogeneous gel-like structure of the suspension. On the other hand, the reference sample 1, derived from direct pulp treatment, shows little to no response to the increase in fluidising in respect to the LVE region at the limited consistency of 1.5 % and illustrates the dominating role of residual fibres in determining the elastic structure, forming entangled flocs [40, 43, 56]. The decade of magnitude difference between the viscoelastic moduli ( $G' \approx 10 G''$ ) seen throughout in Figure 6, even at the low 1.5 % feed consistency for all fluidising passes (1, 2, and

Sample	DP	$M_w$ /kg.mol <sup>-1</sup>	Volume-based median particle size $d_{50v}$ / $\mu\text{m}$	Crystallinity index, CI	Crystallite thickness (size) /nm	Specific surface area (SSA) BET /m <sup>2</sup> g <sup>-1</sup>
1 => Ref (direct from fibre)	1311.7	459.1	800.0 (Kajaani)	0.70	3.5	40.2
2 => MCC (Avicel)	264.3	62.4	58.4	0.79	4.0	0.9
3 => MCC DP390-wet	392.4	156.8	64.6	0.77	4.0	13.1
4 => MCC DP390-dry	389.5	150.8	26.3	0.80	3.9	1.0

Table 1: Raw materials: molecular and structural characteristics.

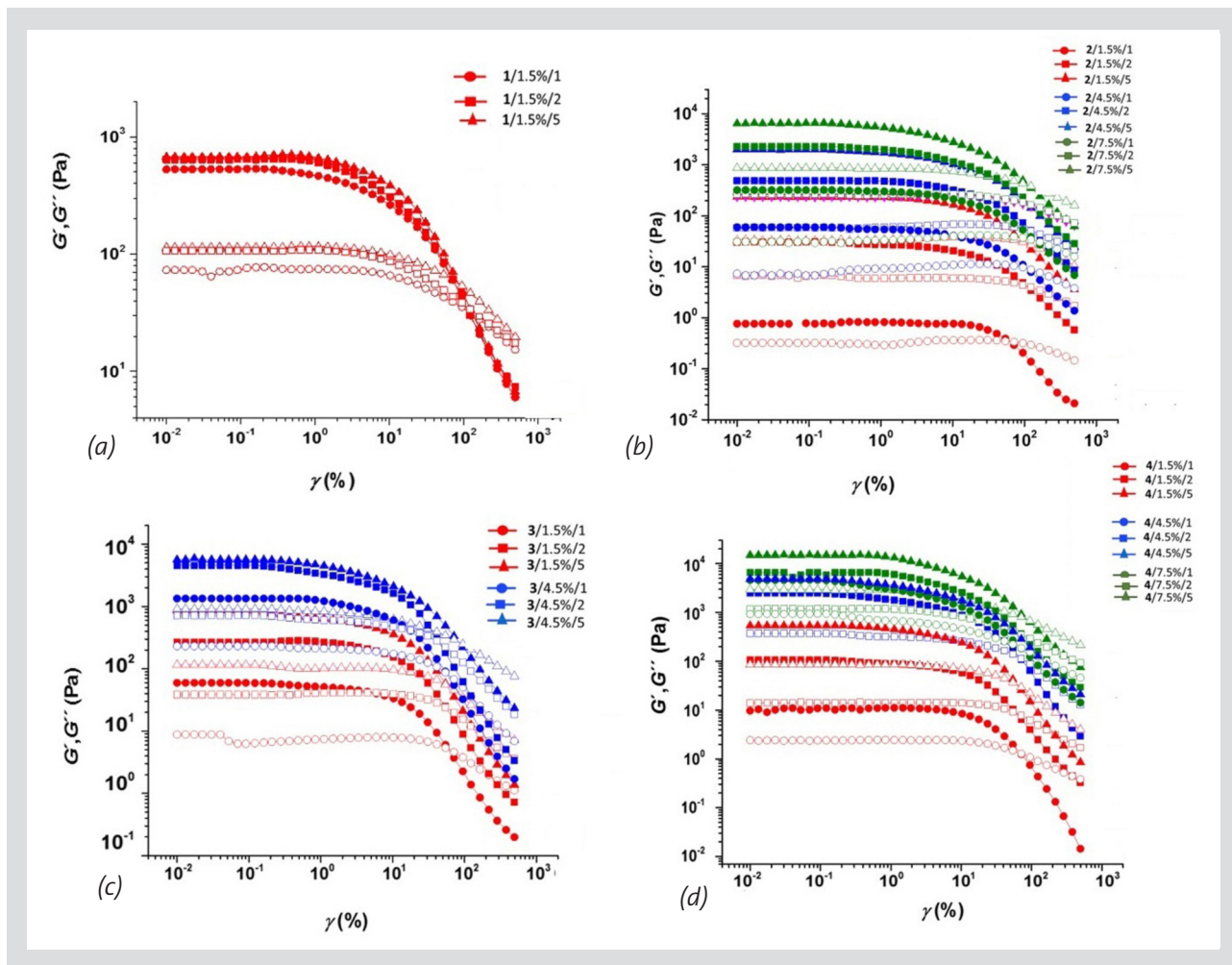


Figure 6: Elastic and storage moduli ( $G'$  and  $G''$ ) of aqueous suspensions of the various feed materials through increasing fluidising steps (1, 2, and 5) and increasing consistency as a function of strain amplitude: (a) Reference 1, (b) commercial MCC 2, (c) DP390-wet MCC 3, and (d) DP390-dry 4 (elastic modulus  $G'$  = closed symbols, loss modulus  $G''$  = open symbols).

5) is explained with respect to the combination of high colloidal stability derived from mutual charge repulsion and the combination of surface adsorbed and trapped water structure. For the MCC feed materials 2, 3, and 4, the magnitude of the moduli increases as a function of mechanical work input (number of passes and consistency increase) until a plateau is reached, after which there is not much change in the viscoelastic response. This can be readily related to the level of fibrillation [11, 12, 41]. Once again, in the case of the reference sample feed 1, no such response is seen at the limited feed solids of 1.5%. The blocky particle morphology of the commercial dried MCC 2, as expected, leads to the lowest starting moduli values [3, 19].

The relative responses of the furnishes, therefore, regarding the degree of fluidising, and the resulting fibrillation generates a progressive increase in gelation of the fibrillated suspension matrix [3, 13, 56]. Deriving fibrils from MCC instead of from fibre-retaining feed material, enables work to be applied directly to the function of specific surface (SSA) rather than energy being lost overcoming the mechanical elastic structure associated with entangled retained fibres [55, 57]. By adopting spray dried MCC, with its lower starting viscosity

compared to the never dried material, not only can solids content be raised, but the initial energy input to direct nanofibrillation will be somewhat greater [54, 56]. These viscoelastic properties in Figure 6 correlate well with the product electron micrographs previously discussed in Figures 4 and 5.

We can follow a similar behavior in respect to the viscoelastic moduli as a function of applied frequency (Figure 7b and c). Progressive increase in fluidising, and thus related particle size decrease, is reflected in the reduction in both  $G'$  and  $G''$  for the all samples as discussed above. Feeding consistency dependence is seen through the difference in gel-structure between the 1.5 and 7.5% dry MCC material products as frequency increases (Figure 7b). As loss moduli is frequency dependent for flocculated suspensions, this is good indicator of flocculation/immobilisation within the matrix as the particles are forced to respond to ever faster oscillatory motion, at higher feed consistency, enabled by using dry MCC feeds, and increase in fluidising steps,  $G'$  and  $G''$  remain constant, independent of frequency [11, 32]. This behavior is indicative of the greater gel-like properties resulting from the increased number of finer fibrils (Figures 7b and c). As can be seen for the DP390 feeds

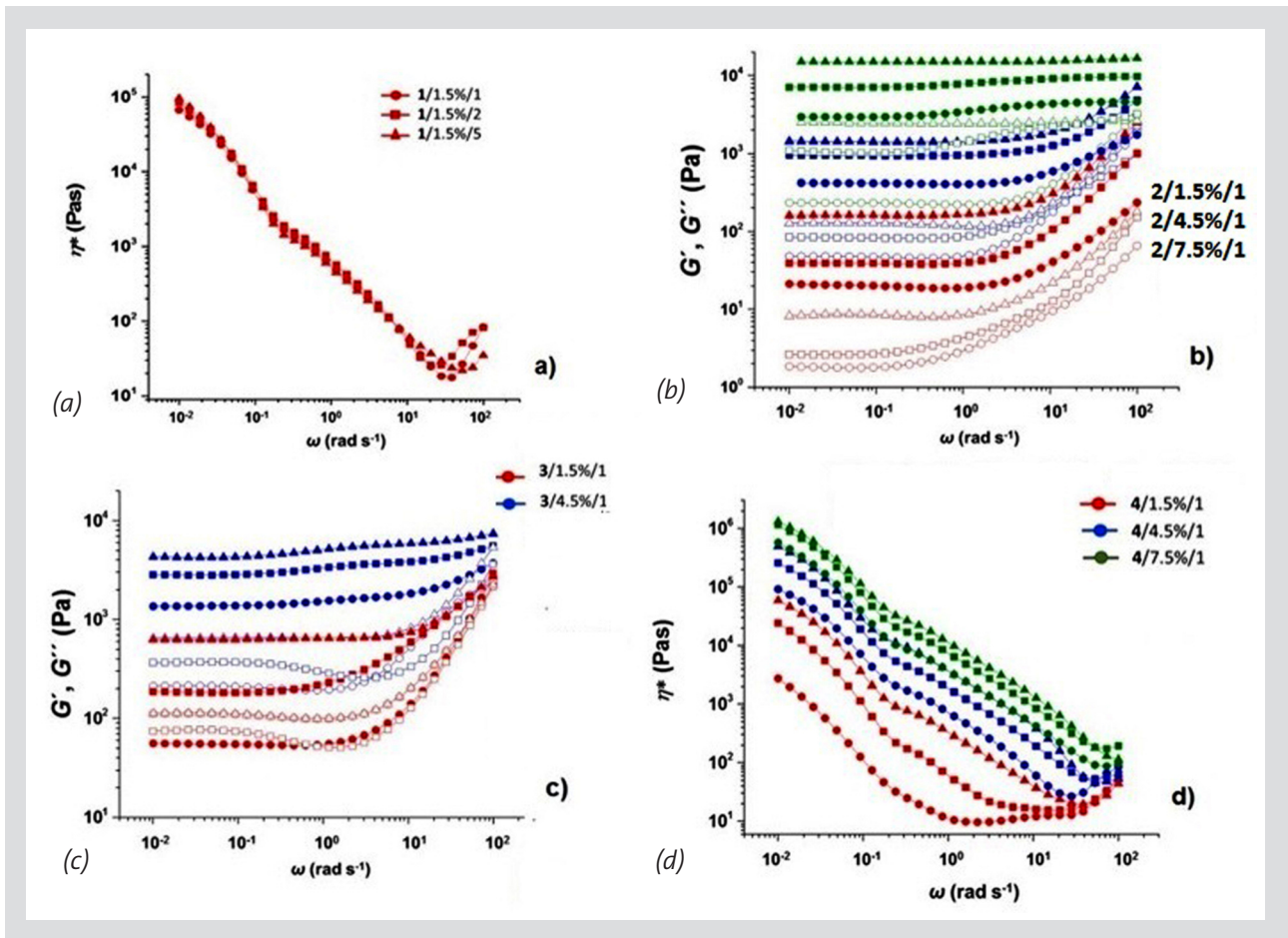


Figure 7: Response of  $G'$  and  $G''$  against frequency ( $\omega = 0.1 - 100 \text{ rad/s}$ ) for all feed consistencies possible for each given feed suspension (1.5, 4.5, and up to 7.5 %) and fluidising steps (1, 2, and 5): (b) Commercial dry MCC 2 at 1.5, 4.5, and 7.5 %, (c) never dried DP390-wet 3 refined at 1.5 and 4.5 %. Elastic modulus  $G'$  is shown as closed symbols, loss modulus  $G''$  as open symbols. Complex viscosity curves for fluidised suspensions  $\eta^*$  as a function of angular frequency  $\omega$  presenting shear thinning behavior as a function of feed material, consistency, and fluidising step: (a) Ref feed 1 and (d) spray dried DP390-dry.

in Figures 7c and d, the effect is consistent with results shown previously in Figures 6c and d, in that the elastic modulus  $G'$  for highly fibrillated material generally remains constant over the frequency range, as the more water trapping the fibrillar material, the more dispersed and gel-like the suspension. The never dried MCC, DP390-dry, could not be run through the fluidiser at the highest solids content of 7.5 % achieved by the dried MCCs and was limited to 4.5 % [33]. This is a process viscosity indicator, reflecting the presence of finer fibrils on the surface, which increases the effective volume fraction. The commercial MCC 2, due to the absence of fibrillation on the particle surface, enables higher initial packing density, and so displays a greater dependency of  $G''$  as fluidising proceeds, creating the finer fibrils [56, 57].

### 3.2.2 Shear thinning behavior

The plots of dependence of complex viscosity  $\eta^*$  on angular frequency  $\omega$  are also shown in Figures 7a and d. We can see that all the suspensions are shear thinning, indicating the rupture of the structural interactive component(s) as the deformation rate increases and is typical for nanofibril suspensions. In Figures 7a and d, the

higher the feed consistency, the greater the decrease in complex viscosity  $\eta^*$  accompanying the increase in fluidising. However, at lower feed consistency the reverse occurs, since the viscosity is low at the lower feed solids but, as the fibrillation proceeds, the viscosity rises to equal that of the higher solids processing, displaying that the system converts to a particle number dependency of fine water-binding material, i.e. greater volume fraction. All flow curves show power-law decay behaviour, i.e. they take the form of Equation 7. The results of fitted shear thinning coefficient  $n_c$  and flow consistency index  $k_c$  show weak dependence on the feed consistency, but if we artificially set  $n_c = -1$  for all suspensions the values of  $k_c$  decrease with increase in feed consistency and fluidising, in agreement with some earlier work [36, 43]. The higher the feed consistency to the fluidiser, the topmost solids being possible for the dried MCC samples showing hornification, together with increasing fluidising steps, the greater the number of material particles that are generated [55, 57]. As the particle number increases, the particle size decreases, and at the extreme case the aspect ratio increases dramatically as the fibrils become thinner as was shown in the SEM micrographs of Figure 4 [18, 38, 40].

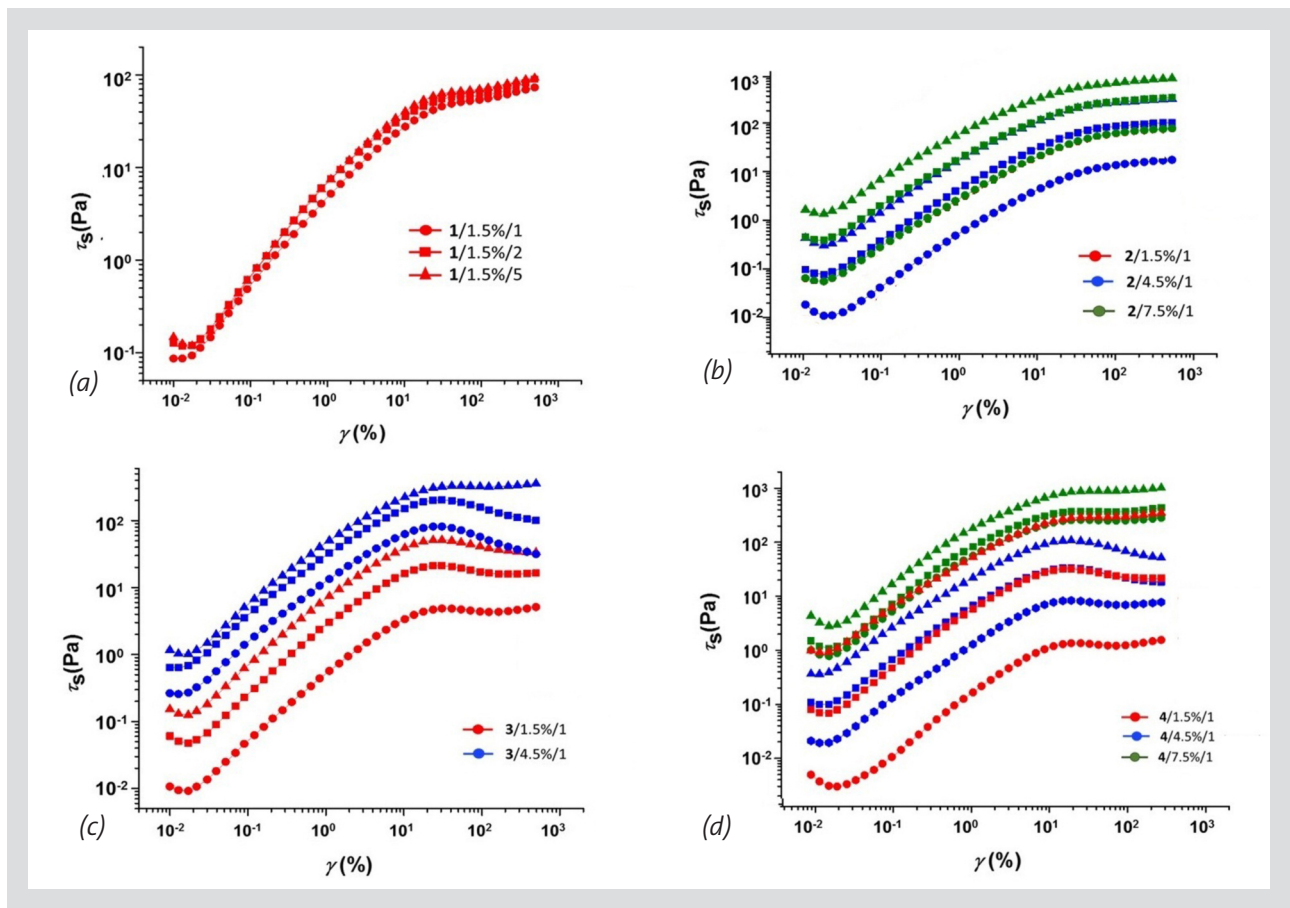


Figure 8: Static stress  $\tau_s$  response to increasing strain amplitude showing static yield stress  $\tau_s^0$ . Stress is reported according to feed consistency (1.5, 4.5, and up to 7.5 %) and the three fluidising levels (1, 2, and 5 passes): (a) Ref-derived samples 1 at 1.5 % feed consistency, (b) commercial powder MCC-derived samples 2, (c) never dried DP390-wet 3, and d) spray dried DP390-dry 4.

### 3.2.3 Static stress behavior

The structuration within the furnish matrix increases the span of static stress values as a function of strain until the breakdown starts at the plateau critical yield stress value  $\tau_s^0$  as the combined structure derived from both mechanical agglomeration, flocculation, and entrapped water within the fibrillar network increases the stress response of the material (Figure 8) [38, 40]. This behavior is dependent on fibril morphology and evident as the aspect ratio is increased by increased fluidising as finer fibrils are released, and the feed consistency further promotes this effect. The electrostatic component of the interaction is manifest in the long range colloidal interaction, and the structural entanglement occurs between the longer elements, most prevalent in the reference-derived fibre-containing samples compared with shorter and finer fibrils derived from MCC, especially at higher feed consistency (Figures 8b and d). The stronger gel-like behavior is produced by the more pronounced water hydrogen bonding within the suspension at high surface area in the dispersed wet state, resulting in further increased effective volume fraction [31, 36, 44]. This reinforced structure accounts for the high yield point in the suspensions [32]. The apparent yield stress of all suspensions increases with the amount of fluidising, additional expressed through increase in feeding consistency [17, 23].

### 3.2.4 Structure recovery after shear

Higher fibrillation decreases the time it takes for the structure to regain its original thixotropic nature [12, 52]. This is shown in respect to the transient viscosity recovery  $\eta^+$  in the third interval of the three interval thixotropy test (3ITT), following previous shear thinning during second high shear interval (Figure 9). This rheopectic recovery behaviour, seen at constant shear rate, can result in an over-shoot peak upon eventual cessation of shear. To trace the over-shooting behavior of structure recovery in the third interval, we reduce the values of  $\eta^+$  with the value of the initial dynamic viscosity in the first interval  $\eta_0$ . An important conclusion regarding the structure recovery after high shear (Figure 9) is that the transient viscosity recovery  $\eta^+$  after high shear is very fast for highly fibrillated material, indicating the number of fibril-fibril interactions and their mobility define the rate of structure recovery. However, the less fluidised samples, especially those containing larger fibre remnants (Ref 1), display greater thixotropy, such that after shear thinning, it is not possible to recover the full starting structure under continuous very low shear, indicating that the particle mobility is limited and the system needs a longer time in a completely static state to recover the full stationary agglomeration which was broken down under shear [51, 56].

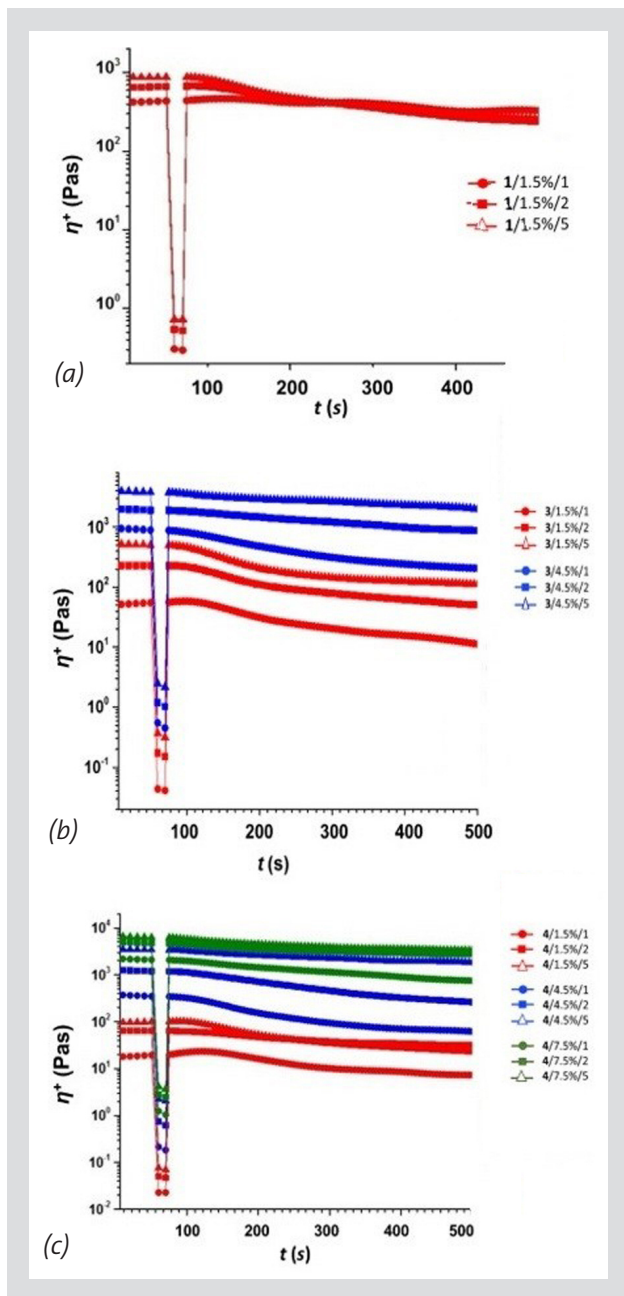


Figure 9: Transient viscosity  $\eta^+$  as a function of time in the three intervals in the low/high/low shear regime obtained from the 3ITT procedure, with inserts in presenting normalised transient viscosity  $\eta^+/\eta_0$ , where  $\eta_0$  is the initial dynamic viscosity in the first low shear interval: (a) Ref sample 1, (b) commercial powder MCC 2, (c) never dried DP390-wet 3, and (d) spray dried DP390-dry 4.

### 3.2.5 Parameterising the flow response

To compare the different response of complex  $\eta^*$  we use iterative least squares methods to reveal the behavior of the flow coefficient  $k_c$  for each sample, together with the respective fitted values for shear thinning index  $n_c$  where the values are reported as  $-(n_c - 1) = 1 - n_c$  (Equation 7). Two separate fits are made for the two regions of shear thinning, i.e. on either side of the transition turning point and yielding values of  $\{k_{c1}, n_{c1}\}$  and  $\{k_{c2}, n_{c2}\}$ . We see in most cases that  $k_{c1}$  is larger for the more agglomerated furnish-derived material that contain

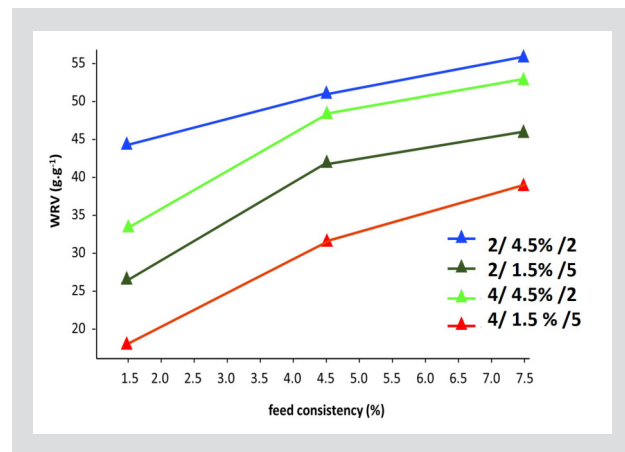


Figure 10: Progressive increase in water retention (decrease of WRV value) of samples as a function of increasing feeding consistency and number fluidising cycles illustrated for the two dry MCC sample feeds, namely 2 commercial MCC and 4 AaltoCellTM DP390-dry.

the less fibrillated product [51, 52]. This observation contrasts with the reduced agglomeration/flocculation for samples derived from the spray dried MCCs 2 and 4, Avicel and AaltoCell DP390-dry, with the never dried DP390-wet falling between the dry MCCs and the fibrous reference system [32, 56]. The suspected change in morphology of spray dried AaltoCellTM-derived samples is supported by the light transmittance (inversely proportional to turbidity), Table 2 and seen in respect to the more gel-like suspension arising from the “hair-like” nanofibrils on the particle surface [45, 50].

### 3.3 CORRELATION WITH WATER RETENTION VALUE

A thorough description of the water binding behavior of a fibrillar cellulose gel should include both the water trapped within the fibrillar network and the water immobilised around and on the surface of the particles [51, 57]. As presented in Figure 10, the WRV data demonstrate the water trapping nature (reducing WRV value) of the more fibrillated materials following 5 passes through the fluidiser and the increase in the gel-build. These WRV results correlate with data obtained from rheological experiments and the fibrillation level can be seen in the SEM images (Figure 4). Increasing fluidising cycles and raising feed consistency using MCC as the start material results in higher water retention, correlating for each feed with the increase in transmittance and finer fibril structure. Initially, spray drying MCC reduces the water retention of the feed material, related clearly to the hornification and reduced SSA, but the ability to fluidise at higher consistency results in greater end-product fibrillation and so the highest water retention values (lowest WRV values) are then obtained [36, 37, 51, 56].

Sample	$\tau_s^0$ /Pa	$G'/G''$ @ $\gamma = 0.12\%$	$G'/G''$ @ $\omega = 0.13$ $\text{rad s}^{-1}$	$1-n_{c1}$ ( $\eta^*/$ Pa.s)	$k_{c1}$ ( $\eta^*/$ Pa.s)	$1-n_{c2}$ ( $\eta^*/$ Pa.s)	$k_{c2}$ ( $\eta^*/$ Pa.s)	$3ITT_{300}$ /s ( $\eta^*/$ Pa.s)	Transmittance $T/\%$			
									$\lambda/\text{nm}$			
									400	600	800	1 000
1/1.5%/1	54.70	5.90	7.20	0.89	17.68	0.40	22.24	0.95	6.37	14.21	21.64	28.04
1/1.5%/2	63.70	6.20	7.50	0.91	13.45	0.52	15.20	0.66	5.73	15.83	26.21	35.15
1/1.5%/5	71.12	7.40	8.10	1.05	9.67	0.61	10.93	0.51	10.20	27.10	41.10	51.00
2/1.5%/1	0.90	3.30	5.40	0.84	9.54	0.57	10.78	0.99	3.50	4.80	5.97	7.21
2/1.5%/2	8.20	4.20	6.10	1.12	8.12	0.80	9.18	1.00	3.70	5.90	8.20	11.00
2/1.5%/5	494.70	7.10	8.90	1.20	6.43	-	7.27	0.84	13.90	24.30	33.50	41.50
2/4.5%/1	18.10	8.20	8.50	1.01	5.45	0.44	6.16	0.92	3.50	4.90	6.10	7.30
2/4.5%/2	105.30	8.40	9.10	1.10	4.56	0.70	5.15	0.87	3.60	5.80	8.10	10.80
2/4.5%/5	347.20	8.90	10.20	1.20	3.56	-	4.02	0.84	6.10	11.60	17.80	24.30
2/7.5%/1	80.10	4.90	5.70	1.12	2.34	-	2.64	0.85	3.90	5.50	7.0	8.50
2/7.5%/2	347.20	7.60	8.10	1.14	2.13	-	2.41	0.81	2.90	4.80	6.80	9.30
2/7.5%/5	862.10	8.60	9.50	1.20	1.56	0.14	1.76	0.80	3.90	7.30	11.50	16.70
3/1.5%/1	8.86	7.10	4.40	0.87	12.89	0.58	14.57	0.51	9.60	12.70	15.80	18.90
3/1.5%/2	21.30	7.40	5.30	0.96	11.56	-	13.06	0.44	13.80	20.60	25.70	30.00
3/1.5%/5	50.10	8.10	5.90	1.02	9.23	0.43	10.43	0.36	31.30	45.60	54.30	60.20
3/4.5%/1	81.40	5.70	4.50	0.91	8.63	0.48	9.75	0.48	8.80	12.40	15.30	17.80
3/4.5%/2	203.20	6.10	5.20	1.04	8.23	-	9.30	0.73	8.40	13.30	17.60	21.50
3/4.5%/5	328.60	6.90	6.50	1.21	6.89	-	7.79	0.74	12.70	21.10	27.80	33.70
4/1.5%/1	1.30	4.20	3.50	0.92	10.11	-	11.42	0.76	7.90	10.10	11.60	13.70
4/1.5%/2	31.80	5.30	4.10	0.96	9.12	-	10.31	0.70	8.10	11.80	15.00	17.80
4/1.5%/5	248.90	7.10	5.30	1.04	8.34	-	9.42	0.47	22.50	34.80	43.10	49.40
4/4.5%/1	8.20	5.80	6.50	0.89	7.85	-	8.87	0.38	8.50	10.90	12.80	14.40
4/4.5%/2	33.70	6.50	6.90	0.94	7.12	-	8.05	0.54	7.50	11.40	14.50	17.40
4/4.5%/5	108.30	6.70	4.90	1.03	5.56	-	6.28	0.73	8.00	14.20	19.70	24.70
4/7.5%/1	17.80	5.10	5.60	1.02	4.56	-	5.15	0.66	7.90	10.40	12.20	14.00
4/7.5%/2	368.40	5.50	6.40	1.10	4.43	-	5.01	0.71	7.30	10.20	12.60	15.00
4/7.5%/5	874.82	5.90	6.40	1.20	3.45	-	3.90	0.68	8.30	13.50	18.00	22.10

Table 2: Summary of the collected data and their parameterisation, providing comparison of the effective rheological behavior obtained from oscillatory and structure recovery measurements, together with light transmittance values at wavelengths  $\lambda = 400, 600, 800, \text{ and } 1000 \text{ nm}$ .

## 4 CONCLUSIONS

Particle size and electron microscopy of fibrillated cellulose materials derived from a comparative series of feed materials undergoing high-pressure fluidising showed that thinner more crystalline cellulose nanofibrillar material can be derived from microcrystalline cellulose (MCC) compared with traditional enzymatic treated mechanical homogenised fibre pulp yielding micro nanofibrillated fibres (MNFC and NFC). The degree of fibrillation, its state of dispersion and the binding behavior of the cellulose surface for water, forming

a gel-like structure, could be clearly followed using rheological procedures focusing on the viscoelastic and complex viscosity properties, reflecting colloidal structure and its breakdown, respectively. Rheological analysis can, therefore, be considered a suitable technique to determine product form constancy. Using the spray dried MCC obtained via the AaltoCell™ process, derived from softwood Kraft pulp, it was confirmed to enable a five-fold solids increase to be applied during fibrillation, as predicted by rheological analysis, compared with a traditional reference consisting of enzymatic pre-treated pulp fibre-derived feed.

## APPENDIX

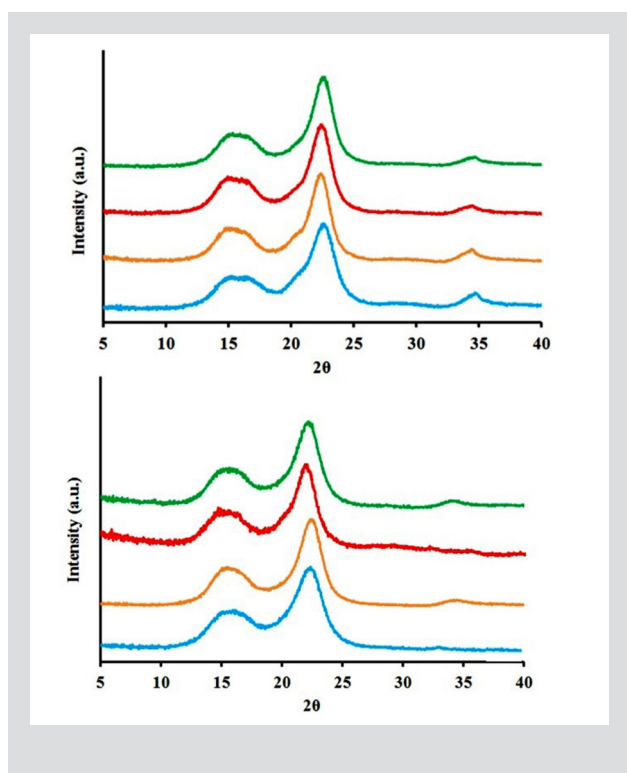


Figure A1: X-ray diffraction patterns of raw materials (a) and microfibrillated celluloses in 1.5% consistency after pass 5 (b): Ref. (blue), Avicel (orange), DP390 (red), and DP390-dry (green).

## REFERENCES

- [1] Klemm D, Kramer F, Moritz S, Lindström T, Ankerfors M, Gray D, Dorris A: Nanocelluloses: a new family of nature-based materials, *Angew. Chem. Int. Ed.* 50 (2011) 5438–5466.
- [2] Moon R J, Martini A, Nairn J, Simonsen J, Youngblood J: Cellulose nanomaterials review: structure, properties and nanocomposites, *Chem. Soc. Rev.* 40 (2011) 3941–3994.
- [3] Hubbe MA, Tayeb P, Joyce M, Tyagi P, Kehoe M, Dimic-Misic K, Pal L: Rheology of nanocellulose-rich aqueous suspensions: a review, *Bioresources* 12 (2018) 9556–9661.
- [4] Sehaqui H, Zhou Q, Berglund LA: Nanostructured biocomposites of high toughness—a wood cellulose nanofiber network in ductile hydroxyethylcellulose matrix, *Soft Matter* 7 (2011) 7342–7350.
- [5] Qing Y, Sabo R, Zhy J Y, Agarwal U, Cai Z, Wu Y: A comparative study of cellulose nanofibrils disintegrated via multiple processing approaches, *Carbohydr. Polym.* 97 (2013) 226–234.
- [6] Paakko M, Vapaavuori J, Silvennoinen R, Kosonen H, Ankerfors M, Lindström T, Berglund LA, Ikkala O: Long and entangled native cellulose I nanofibers allow flexible aerogels and hierarchically porous templates for functionalities, *Soft Matter* 4 (2008) 2492–2499.
- [7] Herrick FW, Casebier RL, Hamilton J K, Sandberg K R: Microfibrillated cellulose: morphology and accessibility, *J. Appl. Polym. Sci.* 37 (1983) 97–813.
- [8] Spence KL, Venditti RA, Rojas OJ, Habibi Y, Pawlak JJ: A comparative study of energy consumption and physical properties of microfibrillated cellulose produced by different processing methods, *Cellulose* 17 (2010) 835–848.
- [9] Iotti M, Gregersen O, Weiby MS, Lenes MJ: Rheological studies of microfibrillar cellulose water dispersions, *Polym. Environ.* 19 (2011) 137–145.
- [10] Lee SY, Chun S, Kang IA, Park JY: Preparation of cellulose nanofibrils by high-pressure homogenizer and cellulose-based composite films, *J. Ind. Eng. Chem.* 15 (2009) 50–55.
- [11] Gullichsen J, Harkonen E: Medium consistency technology, *Tappi J.* 64 (1981) 69–72.
- [12] Spence KL, Venditti RA, Rojas OJ, Habibi Y, Pawlak JJ: A comparative study of energy consumption and physical properties of microfibrillated cellulose produced by different processing methods, *Cellulose* 18 (2011) 1097–1111.
- [13] Henriksson M, Henriksson G, Berglund LA, Lindström TA: An environmentally friendly method for enzyme-assisted preparation of microfibrillated cellulose (MFC) nanofibers, *Eur. Polym. J.* 43 (2017) 3434–3441.
- [14] Ankerfors M: Microfibrillated cellulose: energy-efficient preparation techniques and key properties, Licentiate thesis, KTH Royal Institute of Technology (2012).
- [15] Ankerfors M, Lindström T: Method for providing a nanocellulose involving modified cellulose fibers, International Patent Application WO 2009126106A1 (2009).
- [16] Saito T, Kimura S, Nishiyama Y, Isogai A: Cellulose nanofibers prepared by TEMPO-mediated oxidation of native cellulose, *Biomacromolecules* 8 (2007) 485–2491.
- [17] Zografis GMJ, Kontny MJ, Yang AY, Brenner GS: Surface area and water vapor sorption of macrocrystalline cellulose. *International journal of pharmaceutics.* 18 (1984) 99–116.
- [18] Yokota H, Okumura Y: Homogenization of microcrystalline cellulose suspension, Japan Patent JP 59120638 (1984).
- [19] Jihua L, Wie X, Wang Q, Chen J, Chang G, Kong L, Su Y, Liu Y: Homogeneous isolation of nanocellulose from sugarcane bagasse by high pressure homogenization, *Carbohydrate Polym.* 90 (2012) 1609–1613.
- [20] Lee SY, Chun SJ, Kang IA, Park JY: Preparation of cellulose nanofibrils by high-pressure homogenizer and cellulose-based composite films, *J. Ind. Eng. Chem.* 15 (2009) 50–55.
- [21] Jacquet N, Vanderghem C, Danthine S, Blecker C, Paquet M: Influence of homogenization treatment on physico-chemical properties and enzymatic hydrolysis rate of pure cellulose fibers, *Appl. Biochem. Biotech.* 169 (2012) 1315–1328.
- [22] Zhang L, Tsuzuki T, Wanf X: Preparation of cellulose nanofiber from softwood pulp by ball milling, *Cellulose* 22 (2015) 1729–1741.
- [23] Thanomchat S, Srikulkit K, Suksut B, Schlarb AK: Morphology and crystallization of polypropylene/microfibrillated cellulose composites, *Int. J. Appl. Sci. Technol.* 4 (2014) 23–34.
- [24] Tuason DC, Krawczyk GR, Buliga G: Microcrystalline cellulose, in Food stabilisers, thickeners and gelling agents, Imeson A (ed), Wiley (2009).
- [25] O'Connor RE, Schwartz JB: Drug release mechanism from a microcrystalline cellulose pellet system, *Pharma. Res.* 10 (1993) 356–36.

- [26] Newman RH: Carbon-13 NMR evidence for cocrystallization of cellulose as a mechanism for hornification of bleached Kraft pulp, *Cellulose* 11 (2004) 45–52.
- [27] Dahl O, Vanhatalo K, Parviainen K: A novel method to produce microcellulose, *International Patent Application WO 2011154600* (2011).
- [28] Leppänen K, Andersson S, Torkkeli M, Knaapila M, Kotelnikova N, Serimaa R: Structure of cellulose and microcrystalline cellulose from various wood species, cotton and flax studied by X-ray scattering, *Cellulose* 16 (2009) 999–1015.
- [29] Sczostak A: Cotton linters: An alternative cellulosic raw material, *Macromol. Symp.* 280 (2009) 45–53.
- [30] Vanhatalo K: A new manufacturing process for microcrystalline cellulose (MCC), PhD Thesis, Aalto University (2017).
- [31] Flourey J, Desrumaux A, Axelos MA, Legrand J, Degradation of methylcellulose during ultra-high pressure homogenisation. *Food Hydrocolloids* 16 (2002) 47–53.
- [32] Vanhatalo K, Dahl O: Effect of mild acid hydrolysis parameters on properties of microcrystalline cellulose, *Biore-sources* 9 (2014) 4729–4740.
- [33] Vanhatalo K, Lundin T, Koskimäki A, Lillandt M, Dahl O: Microcrystalline cellulose property–structure effects in high-pressure fluidization: microfibril characteristics, *J. Mater. Sci.* 51 (2016) 6019–6034.
- [34] Vartiainen J, Pöhler T, Sirola K, Pylkkänen L, Alenius H, Hokkinen J, Tapper U, Lahtinen P, Kapanen A, Putkisto K, Hiekkataipale P: Health and environmental safety aspects of friction grinding and spray drying of microfibrillated cellulose, *Cellulose* 18 (2011) 775–786.
- [35] Park S, Venditti RA, Jameel H, Pawlak JJ: Measurement of fiber hornification using high resolution thermogravimetric analysis, *Proceedings of the TAPPI Engineering, Pulping and Environmental Conference*, Philadelphia, TAPPI Press (2005) 30–35.
- [36] Dimic-Misic K, Puiisto A, Gane P, Nieminen K, Alava M, Paltakari J, Maloney T: The role of MFC/NFC swelling in the rheological behavior and dewatering of high consistency furnishes, *Cellulose* 20 (2013) 2847–2861.
- [37] Dimic-Misic K, Nieminen K, Gane P, Maloney T, Sixta H, Paltakari J: Deriving a process viscosity for complex particulate nanofibrillar cellulose gel-containing suspensions, *Appl Rheol.* 24 (2014) 35616.
- [38] Ewoldt RH, Johnston MT, Caretta LM: Experimental challenges of shear rheology: how to avoid bad data, in *Complex fluids in biological systems*, Springer (2015).
- [39] Dimic-Misic K, Maloney T, Gane P: Effect of fibril length, aspect ratio and surface charge on ultralow shear-induced structuring in micro and nanofibrillated cellulose aqueous suspensions. *Cellulose* 25 (2018) 117–136.
- [40] Fernandez M, Huegun A, Munoz ME, Santamaria A: Non-linear oscillatory shear flow as a tool to characterize irradiated polypropylene/MWCNT nanocomposites, *Appl Rheol.* 25 (2015) 45154.
- [41] Schenker M, Schoelkopf J, Gane P, Mangin P: Quantification of flow curve hysteresis data – a novel tool for characterising microfibrillated cellulose (MFC) suspensions, *Appl Rheol.* 28 (2018) 22945.
- [42] Marchesini FH, Naccache MF, Abdu A, Alick AA, de Souza Mendes PR: Rheological characterization of yield-stress materials: Flow pattern and apparent wall slip, *Appl Rheol.* 28 (2015) 53883.
- [43] Kumar V, Nazari B, Bousfield D, Toivakka M: Rheology of microfibrillated cellulose suspensions in pressure-driven flow, *Appl Rheol.* 26 (2016) 43534.
- [44] Iwamoto S, Abe K, Yano H: The effect of hemicelluloses on wood pulp nanofibrillation and nanofiber network characteristics, *Biomacromolecules* 9 (2008) 1022–1026.
- [45] Peng Y, Gardner D J, Han Y, Kiziltas A, Cai Z, Shabalala MA: Influence of drying method on the material properties of nanocellulose I: thermostability and crystallinity, *Cellulose* 20 (2013) 2379–2392.
- [46] Steele DF, Moreton RC, Staniforth JN, Young PM, Tobyn MJ, Edge S: Surface energy of microcrystalline cellulose determined by capillary intrusion and inverse gas chromatography, *AAPS J.* 10 (2008) 494–503.
- [47] Segal LGJMA, Creely JJ, Martin Jr AE, Conrad CM: An empirical method for estimating the degree of crystallinity of native cellulose using the X-ray diffractometer, *Textil. Res. J.* 10 (1959) 786–794.
- [48] Sunghyun N, French AD, Condon BD, Concha M: Segal crystallinity index revisited by the simulation of X-ray diffraction patterns of cotton cellulose I $\beta$  and cellulose II, *Carbohydrate Polym.* 135 (2016) 1–9.
- [49] Patterson AL: The Scherrer formula for X-ray particle size determination, *Phys. Rev.* 56 (1939) 978–982.
- [50] Kangas H, Lahtinen P, Sneek A, Saariaho AM, Laitinen O, Hellen E: Characterization of fibrillated celluloses. A short review and evaluation of characteristics with a combination of methods, *Nordic Pulp & Paper Res. J.* 28 (2014) 129–143.
- [51] Pääkkönen T, Dimic-Misic K, Orelma H, Pönni R, Vuorinen T, Maloney T: Effect of xylan in hardwood pulp on the reaction rate of TEMPO-mediated oxidation and the rheology of the final nanofibrillated cellulose gel, *Cellulose* 23 (2016) 277–293.
- [52] Dimic-Misic K, Gane PAC, and Paltakari J: Micro- and nanofibrillated cellulose as a rheology modifier additive in CMC-containing pigment-coating formulations, *Ind. Eng. Chem. Res.* 52 (2016) 16066–16083.
- [53] Kvien I, Tanem BS, Oksman K: Characterization of cellulose whiskers and their nanocomposites by atomic force and electron microscopy, *Biomacromolecules* 6 (2005) 3160–3165.
- [54] Kolakovic R, Laaksonen T, Peltonen L, Laukkanen A, Hirvonen J: Spray-dried nanofibrillar cellulose microparticles for sustained drug release, *Inter. J. Pharma.* 430 (2012) 47–55.
- [55] Zimmermann MV, Borsoi C, Lavoratti A, Zanini M, Zattera AJ, Santana RM: Drying techniques applied to cellulose nanofibers, *J. Reinforc. Plast. Composit.* 35( 2016) 628–643.
- [56] Rantanen JJ, Dimic-Misic K, Pirttiniemi J, Kuosmanen P, Maloney TC: Forming and dewatering of a microfibrillated cellulose composite paper, *Bioresources* 10 (2015) 3492–3506.
- [57] Nechyporchuk O, Belgacem MN, Pignon F: Current progress in rheology of cellulose nanofibril suspensions, *Biomacromolecules* 17 (2016) 2311–2320.

